KU Leuven
Department of Mechanical Engineering
Celestijnenlaan 300 - box 2420
B-3001 Heverlee (Belgium)

Proceedings of

ISMA2016

International Conference on
Noise and Vibration Engineering

USD2016

International Conference on
Uncertainty in Structural Dynamics

19 to 21 September, 2016
Editors: P. Sas, D. Moens, A. van de Walle

Pore-size effects in sound absorbing foams with periodic microstructure: modelling and experimental verification using 3D printed specimens

T. G. Zieliński[1]

[1] Institute of Fundamental Technological Research of the Polish Academy of Sciences,
ul. Pawińskiego 5B, 02-106 Warsaw, Poland
e-mail: **tzielins@ippt.pan.pl**

Abstract

Microstructure-based modelling of sound absorbing porous media has been recently successfully applied for various materials, however, still some questions concerning the reliability and accuracy of such predictions are open. These issues are investigated here for periodic foams with open porosity. First, a geometry of foam microstructure is generated using an algorithm which ensures periodic arrangements of pores in a cube. Then, the cube is appropriately scaled to various sizes and for each size case finite-element analyses are performed on the periodic fluid domain to calculate the so-called transport parameters. Finally, the effective speed of sound and density are determined for the so-called equivalent fluid, macroscopically suitable to describe wave propagation in such an open rigid foam filled with air. All this allows to estimate the sound absorption for periodic foam layers of various pore-sizes and thicknesses. This parametric study is confronted with some impedance-tube measurements carried out for a few foam samples produced using 3D-printing technology.

1 Introduction

Estimations of wave propagation and attenuation in porous media with rigid frame and fully open porosity can be done using the so-called Johnson-Champoux-Allard (JCA) model [1–3] or its enhanced versions with improvements proposed by Lafarge *et al.* [4] and/or Pride *et al.* [5]. The most elaborated version is the so-called Johnson-Champoux-Allard-Pride-Lafarge (JCAPL) model [6] which uses 8 parameters [1, 6, 7], namely: (1) the open porosity, (2) the so-called tortuosity, (3) the permeability (i.e., the classic porous material parameter known from the Darcy's law), (4) the thermal analogue of permeability (introduced by Lafarge *et al.* [4]), (5) the viscous characteristic length related to viscous drag forces, (6) the thermal characteristic length pertaining to thermal effects, (7) the viscous 'static' tortuosity ('static', i.e., at frequency tending to zero), and (8) the thermal 'static' tortuosity. These parameters are some sort of average, macroscopic projection of crucial microscopic features of porous geometry, and they are sometimes called the transport parameters. Obviously, apart from these purely geometric transport parameters pertaining to the solid part of porous material, some essential properties of fluid in pores are also required by the models. Typically, the following fluid parameters are used [1, 7]: the density, the kinematic viscosity, the Prandtl number, the ratio of specific heats, and the bulk modulus which is directly related to the ambient mean pressure. All these parameters are well known for common fluids and in the most needful case of air also correcting formulas have been developed for some of parameters with respect to the ambient mean pressure, temperature and humidity, which should be carefully measured before commencing any experimental tests. Finally, thanks to the carefully determined density and bulk modulus of air (or other fluid filling the pores) the corresponding speed of sound and characteristic impedance can be determined and used in calculations based on experimental measurements.

A large number of parameters used by the Johnson-Champoux-Allard and other related models is a consequence of the well-founded derivations based on the physical considerations which take into account both, viscous and thermal effects. On the other hand, all this entails a wide versatility of these models which, in principle, can be applied to rigid porous media of any kind, that is, for example, open foams, fibrous materials, and granular media, provided that their transport parameters can be determined. Moreover, the family of Johnson-Champoux-Allard-Pride-Lafarge models forms also a background for modelling of acoustic wave propagation and absorption in poro-elastic media where the adapted Biot's theory is applied [1, 8].

Of the utmost importance is therefore the fact that all transport parameters can be calculated from porous microstructure. To this end, however, a periodic volume element (or sometimes even only a two-dimensional cell) representative for the investigated porous medium is required. Such microstructure-based approach has been applied to various porous materials, like foams [9–16], fibrous materials [17–19], or granular media [7, 20, 21], and recently even to poroelastic materials [22–24]. The transport parameters can be identified using techniques of inverse characterisation, where the microstructure-based investigations may also be involved [15, 25].

This work presents some preliminary investigations concerning the reliability and accuracy of the microstructure-based predictions focusing mainly on the micro-geometric size effects, and the problem of relative size of representative cells with respect to the overall size of porous samples. These issues are investigated for periodic foams with open porosity, wherein a few foam specimens are produced using a 3D-printing technology. The paper is organised as follows. In the next Section a periodic Representative Volume Element (RVE) with 5 pores of different size is proposed and the transport parameters are calculated for various sizes of this RVE by solving some relevant finite element problems on such periodic geometry of foam microstructure. These parameters are then used for the JCAPL model to determine the sound wave propagation and absorption in such foams with various pore sizes. Finally, in Section 3, the results of sound absorption found on the basis of microstructural analyses are compared with some experimental curves of acoustic absorption measured for the 3D-printed foam specimens.

2 Microstructure-based calculations

The algorithm developed in [16] for quasi-random generation of periodic arrangements of pores was used to construct a periodic microstructural geometry of foam with open porosity of 83%. This periodic Representative Volume Element (RVE) forms a cube with 5 pores of various size, where the largest pore is exactly twice as big as the smallest one. Figure 1 presents the periodic skeleton as well as a finite element mesh of the fluid domain inside pores. By scaling the periodic representative cube (i.e., by specifying the length of its edge) the pores get specific sizes: these specific pore diameters are listed in Table 1 for the RVE edge-length from 3 mm to 10 mm. The relative (dimensionless) pore sizes with respect to the largest pore are also presented in this Table.

RVE size:	3	4	5	6	7	7.5	8	9	10	Relative pore size
Pore 1:	2.791	3.722	4.652	5.583	6.513	6.978	7.444	8.374	9.305	1.000
Pore 2:	2.210	2.946	3.683	4.420	5.156	5.525	5.893	6.629	7.366	0.792
Pore 3:	1.861	2.481	3.102	3.722	4.342	4.652	4.962	5.583	6.203	0.667
Pore 4:	1.745	2.326	2.908	3.489	4.071	4.362	4.652	5.234	5.815	0.625
Pore 5:	1.396	1.861	2.326	2.791	3.257	3.489	3.722	4.187	4.652	0.500
Average:	2.001	2.667	3.334	4.001	4.668	5.001	5.335	6.001	6.668	0.717

Table 1: Pore diameters in [mm] (and the average from all 5 pores) in the periodic foam with open porosity 83%, with respect to the RVE size in [mm] (i.e., the edge-length of representative cube); the dimensionless relative pore size is given (in the last column) with respect to the largest pore.
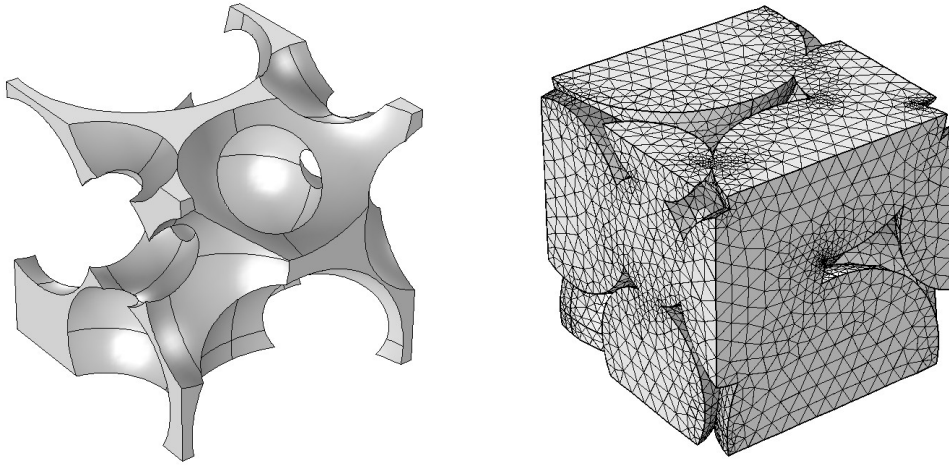
Figure 1: Periodic Representative Volume Element (RVE) with porosity 83%: the solid skeleton and finite element mesh of fluid domain.

RVE size [mm]	(Viscous) permeability [m^2]	Thermal permeability [m^2]	(Inertial) tortuosity [–]	Viscous tortuosity [–]	Thermal tortuosity [–]	Viscous length [mm]	Thermal length [mm]
3	$2.4860 \cdot 10^{-8}$	$9.9422 \cdot 10^{-8}$	1.4424	2.1804	1.4027	0.5545	1.0872
4	$4.4363 \cdot 10^{-8}$	$1.7856 \cdot 10^{-7}$	1.4420	2.1813	1.4077	0.7441	1.4496
5	$6.9356 \cdot 10^{-8}$	$2.8175 \cdot 10^{-7}$	1.4421	2.1968	1.4090	0.9378	1.8120
6	$1.0012 \cdot 10^{-7}$	$3.9763 \cdot 10^{-7}$	1.4421	2.1828	1.4032	1.1232	2.1744
7	$1.3601 \cdot 10^{-7}$	$5.3591 \cdot 10^{-7}$	1.4424	2.1843	1.4000	1.3023	2.5368
7.5	$1.5371 \cdot 10^{-7}$	$6.3715 \cdot 10^{-7}$	1.4424	2.1857	1.4135	1.3973	2.7180
8	$1.7745 \cdot 10^{-7}$	$7.1170 \cdot 10^{-7}$	1.4423	2.1813	1.4059	1.4907	2.8992
9	$2.2472 \cdot 10^{-7}$	$9.0355 \cdot 10^{-7}$	1.4423	2.1856	1.4048	1.6660	3.2616
10	$2.7761 \cdot 10^{-7}$	$1.1538 \cdot 10^{-6}$	1.4421	2.1795	1.4217	1.8756	3.6240

Table 2: Transport parameters for the periodic foam with porosity 83% calculated for various sizes of RVE.

The transport parameters were calculated from microstructure using the periodic RVE scaled to various sizes listed in Tables 1 or 2. To this end, three problems were solved on the fluid domain of periodic RVE with porosity 83%, using the Finite Element Method, namely [7]:

1. the **Stokes problem** – to determine the (viscous) permeability and the parameter of viscous 'static' tortuosity;

2. the **Poisson problem** – to determine the thermal permeability parameter and the parameter of thermal "static" tortuosity;

3. the **Laplace problem** – to determine the (classic, inertial) tortuosity and the viscous characteristic length.

The thermal characteristic length was calculated directly form the microstructural geometry as the double ratio of the fluid domain to the skeleton surface (i.e., the surface of pores).

For the successive microstructure-based calculations, the RVE cube was first scaled so that its edge was from 3 mm to 10 mm (as specified above), and then, finite element meshes were generated on the fluid domain (e.g., see Figure 1) and used for independent numerical analyses to determine eventually the corresponding values of transport parameters. All these values are presented in Table 2. In order to compare the change in value of a parameter with respect to the size of RVE, such relations are plotted in Figure 2 for permeability parameters, in Figure 3 for tortuosity parameters, and Figure 4 for characteristic lengths.
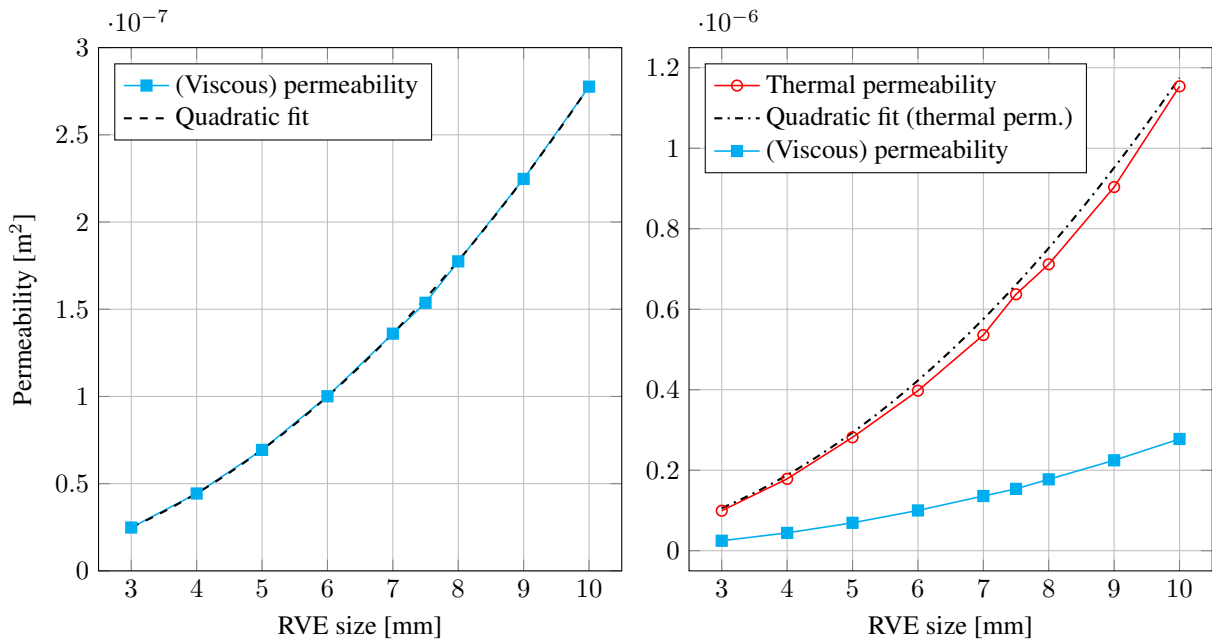
Figure 2: Permeability parameters with respect to the size of periodic RVE.
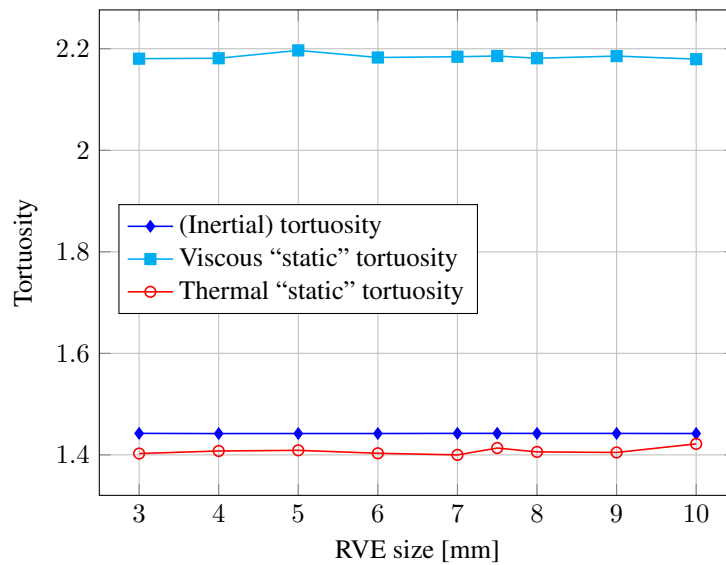

Figure 3: Tortuosity parameters with respect to the size of periodic RVE.

From Table 2 and Figure 3 one can easily observe that whatever is the size of RVE, the toruosity parameters are more or less the same. This observation is very well related to the fact that the tortuosity is essentially related to the shape and not to the size. It is especially visible in case of the classic (inertial) tortuosity parameter where differences scarcely appear at the fifth significant digit. In case of the viscous and thermal tortuosities the discrepancies are more pronounced, although they are still very small (see Figure 3).

The permeability parameters are related to the RVE size in a quadratic manner. Figure 2 presents the viscous and thermal permeabilities with respect to the RVE size as well as quadratic fits for these relations. The quadratic relation found for viscous permeability as: $2.7770 \cdot 10^{-3} \times (\text{RVE size})^2$, is extremely well-fitted, whereas the quadratic relation for thermal permeability, e.g.: $1.1748 \cdot 10^{-2} \times (\text{RVE size})^2$, tends to be slightly approximative (see Figure 2).
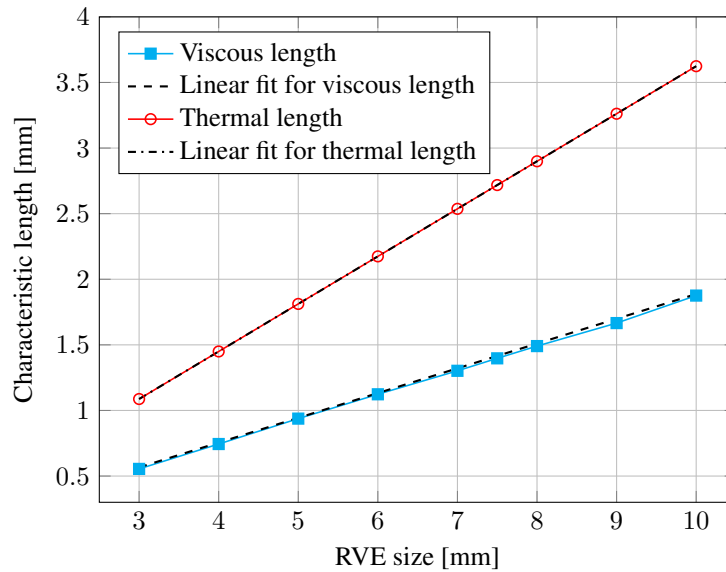
Figure 4: Characteristic lengths with respect to the size of periodic RVE.

The characteristic lengths are linearly related to the RVE size. This is illustrated in Figure 4, where the linear fit for viscous length is: $0.18873 \times$ (RVE size), and the one for thermal characteristic length is: $0.3624 \times$ (RVE size).

The transport parameters calculated from the differently scaled RVE were used for the JCAPL model to determine the frequency-dependent effective speed of sound and density of foams represented by these volume elements. These frequency-dependent characteristics served to solve the problem (governed by the Helmholtz equation) of acoustic absorption by a foam layer of specific thickness (see, for example [25, 26]), in particular, for the layer thickness of 40 mm. These results will be presented and discussed in the next Section.

3   Acoustic absorption of periodic foams

Figure 5 presents three foam samples manufactured using 3D-printing technology. The samples have cylindrical shape with the same diameter of 29 mm and height of 40 mm. The micro-geometry of foam specimens is defined by the periodic RVE was used for finite element calculations on the micro-scale level and shown in Figure 1. Therefore, all samples have the identical shape of skeleton and open porosity of 83%. They differ significantly by the size of pores since for each specimen the representative cubic cell was differently scaled and so different three-dimensional arrays of cells were used to fit the specimen cylinder in (see Figure 6), namely:

- $7 \times 7 \times 8 \times$ periodic cell with 5 mm egde,

- $5 \times 5 \times 5 \times$ periodic cell with 8 mm egde,

- $3 \times 3 \times 4 \times$ periodic cell with 10 mm egde.

Notice that $8 \times 5\,\text{mm} = 5 \times 8\,\text{mm} = 4 \times 10\,\text{mm} = 40\,\text{mm}$ which is exactly the height of specimens, while $7 \times 5\,\text{mm}$ and $5 \times 8\,\text{mm}$ and $3 \times 10\,\text{mm}$ are all larger than their diameter, that is, 29 mm (see also Figure 6).

Figure 7 shows each of the foam samples placed inside the impedance tube with diameter of 29 mm. This equipment was used to measure the acoustic absorption coefficient for each foam specimen using the two-microphone transfer function method, in the frequency range from 500 Hz to 6.4 kHz. The experimental
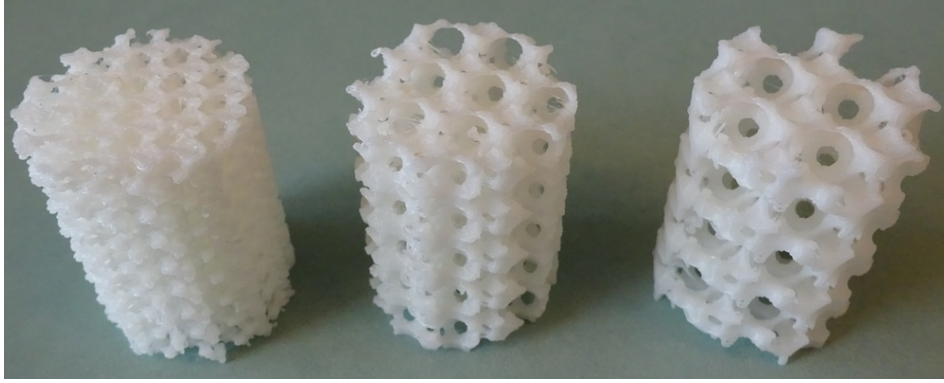
Figure 5: Periodic foam specimens (with porosity 83% and various sizes of periodic cell, namely: 5 mm, 8 mm, and 10 mm) manufactured using 3D-printing technology; the height and diameter for all samples are the same and equal 40 mm and 29 mm, respectively.
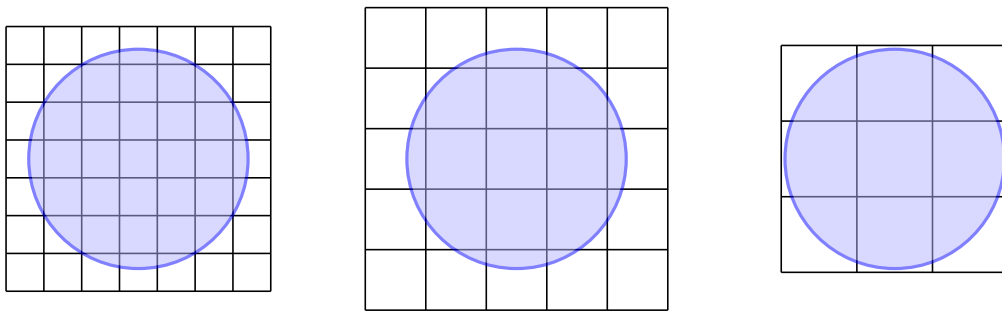

Figure 6: Placement of cylindrical specimens within the arrays of cubic periodic cells of different size (edge-length), namely: $7 \times 7 \times 5$ mm (left), $5 \times 5 \times 8$ mm (middle), and $3 \times 3 \times 10$ mm (right); the diameter of cylindrical specimens is 29 mm.

Figure 7: 3D-printed samples of periodic foam (with porosity 83% and various sizes of periodic cell, namely: 5 mm, 8 mm, and 10 mm) inside the impedance tube with diameter 29 mm.

curves are presented in Figure 8 where they are confronted with the numerical calculations carried out for the cubic RVE with the edge accordingly scaled to 5 mm, 8 mm, and 10 mm, as explained in the previous Section.

A clear although only qualitative compliance is found between the experimental and numerical curves (see Figure 8). It seems that the dispersion effects – responsible for the frequency-dependent maxima/minima and the overall shape of curves – are well predicted by the microstructure-based modelling. On the other hand, the wave attenuation effects are highly underestimated by the results of numerical calculations. There seems to be two main reasons for that, namely:
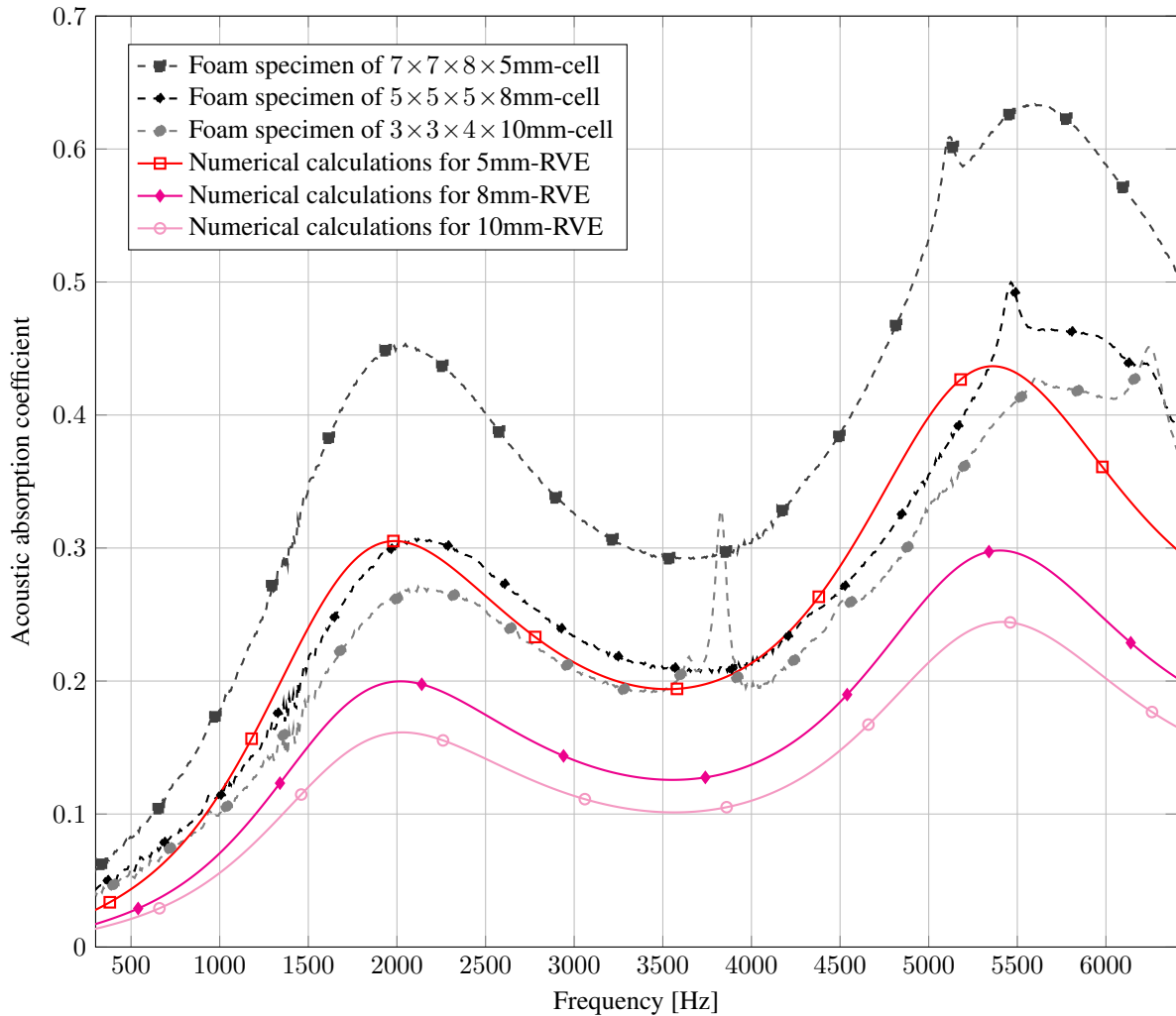
Figure 8: Acoustic absorption

- the separation of scales is not satisfied at all or met very poorly: the periodic cells are fairly large and their size is comparative with the overall size of foam specimens; for example, in case of the specimen with 10 mm-cells only 4 periodic cells are along the sample height and less than 3 of them across the sample diameter; here it should be recalled that there are only 5 complete pores inside the representative cell and the diameter of the largest pore is almost equal to the size of cell, namely, it is 0.93 of the cell edge-length; therefore, in experimental testing some local and inhomogeneous effects appear (like localized 'acute' resonance peaks probably related to the size of the largest pores and slightly dependent on the rotational positioning of the porous surface of sample inside the tube which was manifested through repetitive measurements); moreover, the scattering and other effects – which are completely disregarded in the modelling – should play an important role in wave attenuation;

- the roughness and other imperfections (e.g., tiny plastic fluff and fibres inside pores) of 3D-printed foam specimens are not taken into account in modelling; during measurements, these imperfections strongly increase viscous dissipation effects [27].

4 Conclusions

The following relations exist between the RVE size – and thus, the overall pore size in foam – and the relevant transport parameters:

- a quadratic relation of the permeability parameters to the pore size,

- a linear dependency of the characteristic lengths to the pore size,

- the independence of tortuosity parameters on the pore size.

These relations are fairly precise, therefore, simple scaling formulas – quadratic for the permeability parameters and linear for the characteristic lengths – can be used to determine the change in their values when uniformly modifying the size of porous microstructure. To derive these scaling formulas, one would require only two or three microstructure-based calculations for two or three different sizes of RVE. The tortuosity parameters require only one calculation, because (similarly to the porosity) they are related only to the shape of porous microstructure and independent on its physical sizes.

For the investigated periodic foam and its various sizes, the sound absorption decreased with the overall increase of pore size; the decreasing was uniform in the whole considered frequency range.

The discrepancies in predicted and measured sound absorption (that is, between the results of microstructure-based calculations and experimental tests) seem to be caused by the weak separation of scales (which is a violation of the fundamental assumption) and also by the roughness and imperfections in the 3D-printed foam specimens. Nevertheless, more investigations on that matter are necessary.

Acknowledgements

References

[1] J. F. Allard, N. Atalla, *Propagation of Sound in Porous Media: Modelling Sound Absorbing Materials, Second Edition*, Wiley (2009).

[2] D. L. Johnson, J. Koplik, R. Dashen, *Theory of dynamic permeability and tortuosity in fluid-saturated porous media*, J. Fluid Mech., Vol. 176 (1987), pp. 379–402.

[3] Y. Champoux, J.-F. Allard, *Dynamic tortuosity and bulk modulus in air-saturated porous media*, J. Appl. Phys., Vol. 70 (1991), pp. 1975–1979.

[4] D. Lafarge, P. Lemarinier, J. F. Allard, V. Tarnow, *Dynamic compressibility of air in porous structures at audible frequencies*, J. Acoust. Soc. Am., Vol. 102, No. 4 (1997), pp. 1995–2006.

[5] S. R. Pride, F. D. Morgan, A. F. Gangi, *Drag forces of porous-medium acoustics*, Phys. Rev. B, Vol. 47, No. 9 (1993), pp. 4964–4978.

[6] APMR – Acoustical Porous Material Recipes, `http://apmr.matelys.com/`

[7] T. G. Zieliński, *Microstructure-based calculations and experimental results for sound absorbing porous layers of randomly packed rigid spherical beads*, J. Appl. Phys., Vol 116, No. 3 (2014), Art. No. 034905.

[8] M. A. Biot, *The theory of propagation of elastic waves in a fluid-saturated porous solid*, J. Acoust. Soc. Am., Vol. 28, No. 2 (1956), pp. 168–191.

[9] C. Perrot, R. Panneton, X. Olny, *Periodic unit cell reconstruction of porous media: Application to open-cell aluminum foams*, J. Appl. Phys., Vol. 101 (2007), Art. No. 113538.

[10] C. Perrot, F. Chevillotte, R. Panneton, *Bottom-up approach for microstructure optimization of sound absorbing materials*, J. Acoust. Soc. Am., Vol. 124, No. 2 (2008), pp. 940–948.

[11] C. Perrot, F. Chevillotte, R. Panneton, *Dynamic viscous permeability of an open-cell aluminum foam: Computations versus experiments*, J. Appl. Phys., Vol. 103 (2008), Art. No. 024909.

[12] I. Malinouskaya, V. V. Mourzenko, J.-F. Thovert, P. M. Adler, *Wave propagation through saturated porous media*, Phys. Rev. E, Vol. 77 (2008), Art. No. 066302.

[13] F. Chevillotte, C. Perrot, R. Panneton, *Microstructure based model for sound absorption predictions of perforated closed-cell metallic foams*, J. Acoust. Soc. Am., Vol. 128, No. 4 (2010), pp. 1766–1776.

[14] C. Perrot, F. Chevillotte, M. T. Hoang, G. Bonnet, F.-X. Bécot, L. Gautron, A. Duval, *Microstructure, transport, and acoustic properties of open-cell foam samples. experiments and three-dimensional numerical simulations*, J. Appl. Phys., Vol. 111 (2012), Art. No. 014911.

[15] T. G. Zieliński, *Inverse identification and microscopic estimation of parameters for models of sound absorption in porous ceramics*, in: P. Sas, D. Moens, S. Jonckheere (Eds.), *Proceedings of International Conference on Noise and Vibration Engineering (ISMA2012) / International Conference on Uncertainty in Structural Dynamics (USD2012)*, Leuven (2012), pp. 95–108.

[16] T. G. Zieliński, *Generation of random microstructures and prediction of sound velocity and absorption for open foams with spherical pores*, J. Acoust. Soc. Am., Vol. 137, No. 4 (2015), pp. 1790–1801.

[17] C. Peyrega, D. Jeulin, *Effects of the microstructure of fibrous media on their acoustic properties*, in: *Proceedings of the COMSOL Conference 2010*, Paris (2010).

[18] C. Peyrega, D. Jeulin, *Estimation of acoustic properties and of the representative volume element of random fibrous media*, J. Appl. Phys., Vol. 113 (2013), Art. No. 104901.

[19] T. G. Zieliński, *On representativeness of the representative cells for the microstructure-based predictions of sound absorption in fibrous and porous media*, in: *Proceedings of EuroNoise 2015 – the 10th European Congress and Exposition on Noise Control Engineering*, Maastricht (2015), pp. 2473–2478.

[20] S. Gasser, F. Paun, Y. Bréchet, *Absorptive properties of rigid porous media: Application to face centered cubic sphere packing*, J. Acoust. Soc. Am., Vol. 117, No. 4 (2005), pp. 2090–2099.

[21] C.-Y. Lee, M. J. Leamy, J. H. Nadler, *Acoustic absorption calculation in irreducible porous media: A unified computational approach*, J. Acoust. Soc. Am., Vol. 126, No. 4 (2009), pp. 1862–1870.

[22] T. Yamamoto, S. Maruyama, K. Terada, K. Izui, S. Nishiwaki, *A generalized macroscopic model for sound-absorbing poroelastic media using the homogenization method*, Comput. Methods Appl. Mech. Engrg., Vol. 200 (2011), pp. 251–264.

[23] M. T. Hoang, G. Bonnet, H. T. Luu, C. Perrot, *Linear elastic properties derivation from microstructures representative of transport parameters*, J. Acoust. Soc. Am., Vol. 135, No. 6 (2014), pp. 3172–3185.

[24] K. Gao, J. van Dommelen, P. Göransson, M. G. D. Geers, *A homogenization approach for characterization of the fluid-solid coupling parameters in Biot's equations for acoustic poroelastic materials*, J. Sound Vib., Vol. 351 (2015), pp. 251–267.

[25] T. G. Zieliński, *Normalized inverse characterization of sound absorbing rigid porous media*, J. Acoust. Soc. Am., Vol. 137, No. 6 (2015), pp. 3232–3243.

[26] T. G. Zieliński, *Numerical investigation of active porous composites with enhanced acoustic absorption*, J. Sound Vib., Vol. 330, No. 22 (2011), pp. 5292–5308.

[27] A. Cortis, J. G. Berryman, *Frequency-dependent viscous flow in channels with fractal rough surface*s, Phys. Fluids, Vol. 22 (2010), Art. No. 053603.